Vacuum 155 (2018) 64–72

Contents lists available at ScienceDirect

Vacuum

journal homepage: www.elsevier.com/locate/vacuum

Fast production of high entropy alloys ($CoCrFeNiAl_xTi_y$) by electric current activated sintering system

Azmi Erdogan[a,b], Tuba Yener[c,*], Sakin Zeytin[c]

[a] Bartın University, Engineering Faculty, Metallurgy and Materials Engineering Department, Bartın, Turkey
[b] Sakarya University, Institute of Science and Technology, Sakarya, Turkey
[c] Sakarya University, Engineering Faculty, Metallurgy and Materials Engineering Department, Sakarya, Turkey

ARTICLE INFO

Keywords:
Electric current activated sintering (ECAS)
High entropy alloy (HEA)
Intermetallic
Hardness

ABSTRACT

Electric current assisted sintering (ECAS) can be a new production method for high entropy alloy production due to its advantages such as low sintering temperature and short holding time. In this study, production of CoCrFeNiAlxTiy alloys (x:0.5, y:0,05, 1; y:0.5, x:0, 1) was carried out in electric current activated/assisted sintering system in open air with a uniaxial contact pressure of 35 MPa at 2500 A for 5 min. Microstructural and micro hardness properties of samples are determined. After sintering, depending on the composition, solid solution phases such as FCC (FeNi), BCC (FeCr) were formed in all alloys. In alloys other than $CoCrFeNiAl_{0.5}$, sigma and Al-Ni-Ti intermetallic phases are formed. According to SEM-EDS analyses, the elements with high negative mixing enthalpy are gathered together and the dark phases are enriched from the Al-Ni-Ti, while the Fe-Cr is precipitated due to its high concentration around this phase. Thanks to intermetallic phases formed by the lattice distortion of Al and Ti elements with high atomic radius, the hardness was obtained as 401 H V in $CoCrFeNiAl_{0.5}$ alloy and 700 H V in $CoCrFeNiAl_{0.5}Ti_{0.5}$ alloy. Alloys were subjected to homogenization heat treatment at 1200 °C for 18 h after sintering. As a result of homogenization, the increase in the formation of sigma phase is generally multiplied. While the microstructure distribution became more homogeneous by annealing, an increase in the lattice parameters of the phases was generally observed. Hardness values increased up to 496 H V in the $CoCrFeNiAl_{0.5}$ alloy and 956 H V in the $CoCrFeNiAl_{0.5}Ti_{0.5}$ alloy due to the increase in distortion and high hardness sigma phase due to the increase of the lattice parameters.

1. Introduction

High entropy alloys (HEAs) have attracted extensive research attention in the past decade because of their unusual properties [1–5]. High-entropy alloys (HEAs) are a new class of materials which was first introduced by Yeh et al. and by Cantor et al., in 2004 [6,7]. Unlike traditional alloys, HEAs contain at least five principal elements with each having elemental concentration between 5 and 35 at.% [8–16]. It has been experimentally determined that each alloying element, with its own crystalline structure, atomic ratio and melting point, has a direct effect on the physical and chemical properties of the alloy [17]. The term "high-entropy" is based on the hypothesis that the high mixing entropy of these compositionally complex alloys can overcome the enthalpies of compound formation, i.e., favor the formation of a single solid solution with face-centered cubic (FCC) and/or body-centered cubic (BCC) structures [9,18–24]. The majority of reported HEA compositions are based on the transition metals, namely Co, Cr, Fe and Ni, with addition of elements like Al, Cu, Mn, V, Ti and Mo [9]. However, the CoCrFeNi(x) HEA systems have been prepared mainly by arc melt/casting. But this fabrication route may be unsuitable for industrial manufacturing due to the disadvantages of economy, segregation problem and limitations in shape and size of final products [17,25]. To produce high entropy alloys, the pressure-assisted electric current activated sintering (ECAS) method may be an alternative method. The use of ECAS for consolidating samples not only provides a faster heating time and shorter dwell time but also gives lower sintering temperatures. In this technique, an electric current is applied simultaneously with a mechanical pressure to consolidate or synthesize and to densify specific products into a desired configuration and density [26–31].

With the aim to explore alternative routes to synthesize high entropy alloys and improve their performance, in this work we focused on the high-entropy alloy system of $CoCrFeNiAl_xTi_y$ synthesized by ECAS, and studied on the alloying behavior, microstructure and hardness properties. Furthermore, the main purpose is to produce this kind of alloys in minimum possible time and temperature with ECAS technique. In this way we aimed to save energy consumption for a clean

* Corresponding author.
E-mail address: tcerezci@sakarya.edu.tr (T. Yener).

https://doi.org/10.1016/j.vacuum.2018.05.027
Received 26 March 2018; Received in revised form 16 May 2018; Accepted 17 May 2018
Available online 21 May 2018
0042-207X/

Table 1
Properties of used powders.

Powder	Purity (%)	Particle Size (mesh)
Titanium	99.5	−325
Aluminum	99.5	−325
Nickel	99.8	−325
Cobalt	99.8	−325
Chromium	99	−325
Ferrous	98	−325

Table 2
Process parameters.

Sample code	Wt.%	Current (A)	Voltage (V)	Holding Time (min)
C1	$CoCrFeNiAl_{0.5}$	2500	1.5–2.2	5
C2	$CoCrFeNiAl_{0.5}Ti_{0.5}$	2500	1.5–2.1	5
C3	$CoCrFeNiAl_{0.5}Ti$	2500	1.2–1.6	5
C4	$CoCrFeNiTi_{0.5}$	2500	1.3–1.8	5
C5	$CoCrFeNiAlTi_{0.5}$	2500	1.2–1.7	5

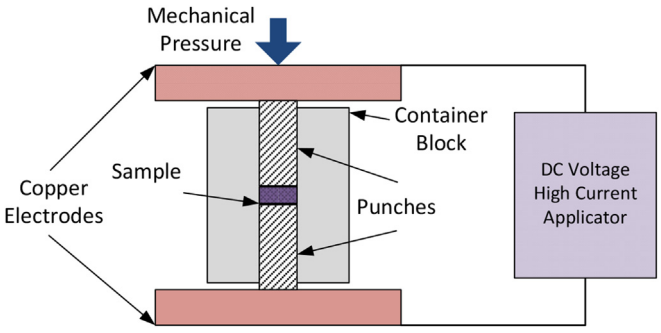

Fig. 1. Schematic presentation of the electric-current-assisted sintering (ECAS) process [28].

environment.

2. Experimental study

High purity Co, Cr, Fe, Ni, Al and Ti powders with particle size less than 45 μm were used as starting materials (Table 1). The alloys with nominal compositions of $CoCrFeNiAl_{0.5}$, $CoCrFeNiAl_{0.5}Ti_{0.5}$, $CoCrFeNiAl_{0.5}Ti$, $CoCrFeNiTi_{0.5}$ and $CoCrFeNiAlTi_{0.5}$ (Table 2) were ball milled for 5 h at 250 rpm in air atmosphere. Methanol was added as a process control agent to inhibit the particle agglomeration. In order to provide the contacts between individual powders in the initial period of the process, the samples were pressed with a die with a compression load of 250 MPa for 1 min. Dimensions of the compact were 15 mm in diameter and 3 mm in thickness. After obtaining the samples, direct electric current (2500 A, 1.2–1.8 V) was applied to the specimen with a pressure of 50 MPa for 5 min using the electric-current-activated sintering technique in an open-atmosphere ECAS system, as shown in Fig. 1. In order to easily remove the sample after sintering, the punches and the specimens were separated by graphite foils of 0.2 mm in thickness. After the sintering, the specimens were unloaded and cooled to room temperature. The sintered alloys were annealed at 1200 °C for 18 h in argon atmosphere to prevent oxidation and cooled in furnace.

The method used in this paper is electric current assisted sintering (ECAS) technique. Here, the electric current is mainly based on the principle of sintering the sample passing through green body compacts or powders, and are generally conducted with simultaneously an additional pressure application. The pressure of 35 MPa is applied to

Table 3
Phases and their lattice parameters of the as-sintered $CoCrFeNiAl_xTi_y$ alloys, in accordance to the XRD analysis.

Alloy	Lattice	Lattice parameters (Å)
$CoCrFeNiAl_{0.5}$	BCC1 (FeCr) FCC (FeNi)	2.879 ± 0.002 3.603 ± 0.003
$CoCrFeNiAl_{0.5}Ti_{0.5}$	BCC1 (FeCr) BCC2 (Al-Ni-Ti) Tetragonal (sigma)	2.881 ± 0.003 2.918 ± 0.002 a = 8.783 ± 0.005, c = 4.557 ± 0.003
$CoCrFeNiAl_{0.5}Ti$	BCC1 (FeCr) BCC2 (Al-Ni-Ti)	2.882 ± 0.002 2.930 ± 0.003
$CoCrFeNiTi_{0.5}$	BCC1 (FeCr) FCC (FeNi) Tetragonal (sigma)	2.883 ± 0.003 3.587 ± 0.003 a = 8.796 ± 0.005, c = 4.563 ± 0.003
$CoCrFeNiAlTi_{0.5}$	BCC1 (FeCr) BCC2 (Al-Ni-Ti)	2.879 ± 0.002 2.931 ± 0.003

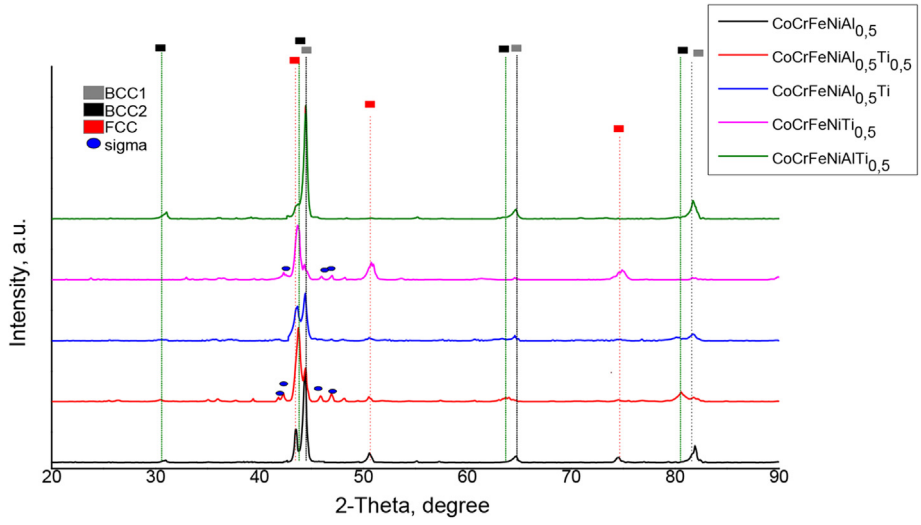

Fig. 2. XRD patterns of the as-sintered $CoCrFeNiAl_xTi_y$ alloys.

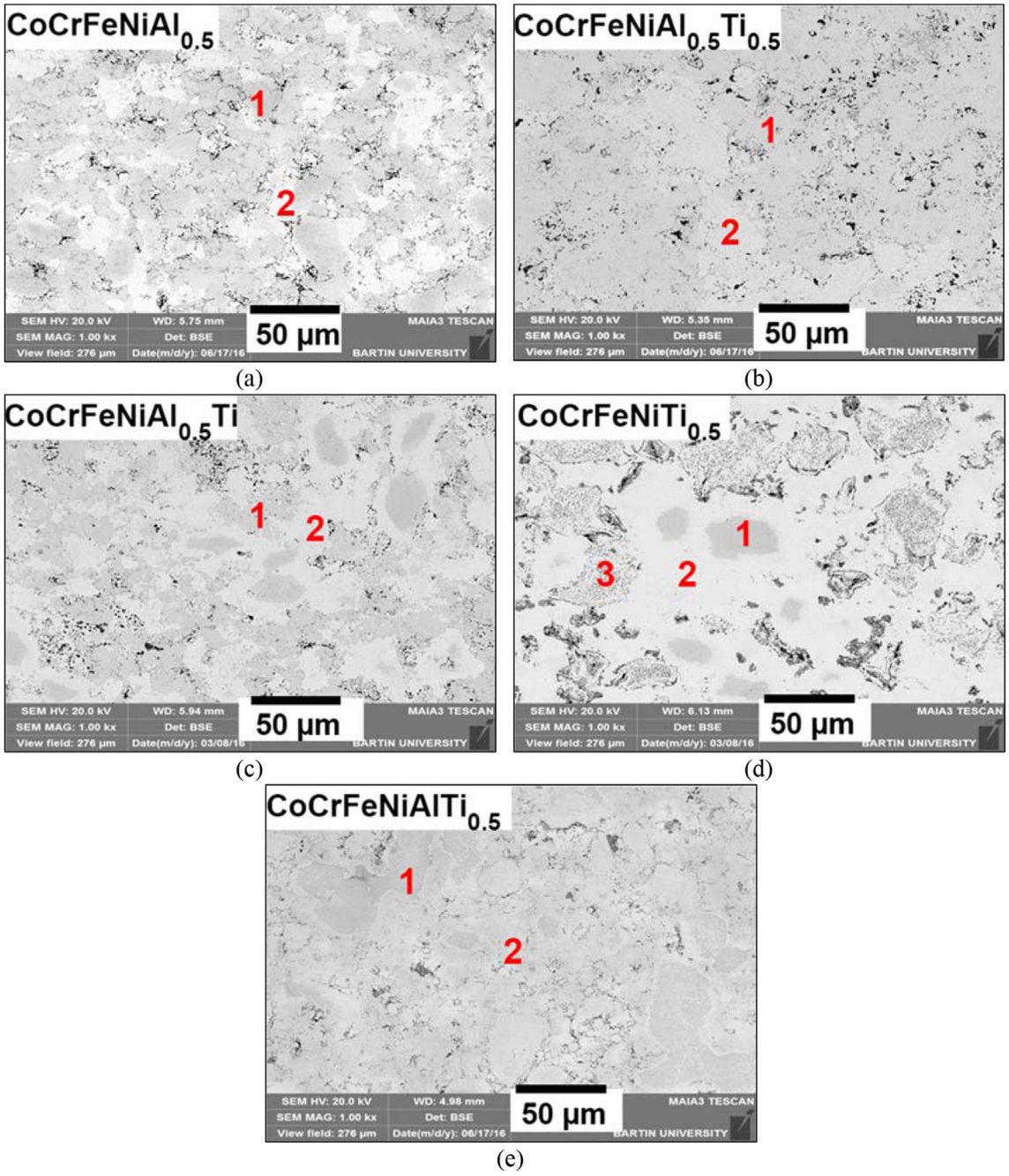

Fig. 3. SEM images of as-sintered $CoCrFeNiAl_xTi_{y.,}$ (a) C1, (b) C2, (c) C3, (d) C4, (e) C5.

provide contact between powders. In this method, the powder or compact material is heated in the container to the desired temperature and then the sintering process is terminated by taking the pressure back. Heat is generated by the Joule effect.

The crystal structure of the as-preserved alloys prepared was examined by X-ray diffractometer (XRD, RIGAKU D/MAX/2200/PC) with a wavelength of 1.5418 A over a 2θ range of 10–80° with CuKα radiation. The microstructures of the alloys were observed using scanning electron microscopy (SEM, TESCAN MAIA3 XMU). Micro hardness measurements were performed using a Vickers microhardness tester (QNESS Q10 M) under a load of 100 g for 10 s. Five measurements were made for each sample to obtain the averaged experimental data.

3. Results and discussion

3.1. XRD analyses as-sintered CoCrFeNiAlxTiy alloys

After ECAS process, XRD patterns, belongs to as-sintered alloys, are shown in Fig. 2, and the identified phases with their lattice parameters are given in Table 3. The phases detected from the XRD patterns are marked in Fig. 2. While the FCC and BCC1 phases are seen in the $CoCrFeNiAl_{0.5}$ alloy, the relative intensity of the BCC1 phase peak is stronger. This indicates that the weight fraction of the FCC phase is smaller than that of the BCC1 phase [8]. The BCC1 phase was also detected in the $CoCrFeNiAl_{0.5}Ti$ alloy with a higher lattice parameter. Differently, BCC2 phase peaks were seen in the alloy with tetragonal sigma phase. In the $CoCrFeNiAl_{0.5}Ti$ alloy, the tetragonal structure sigma phase is not seen. Peaks of BCC1 and BCC2 phases were observed

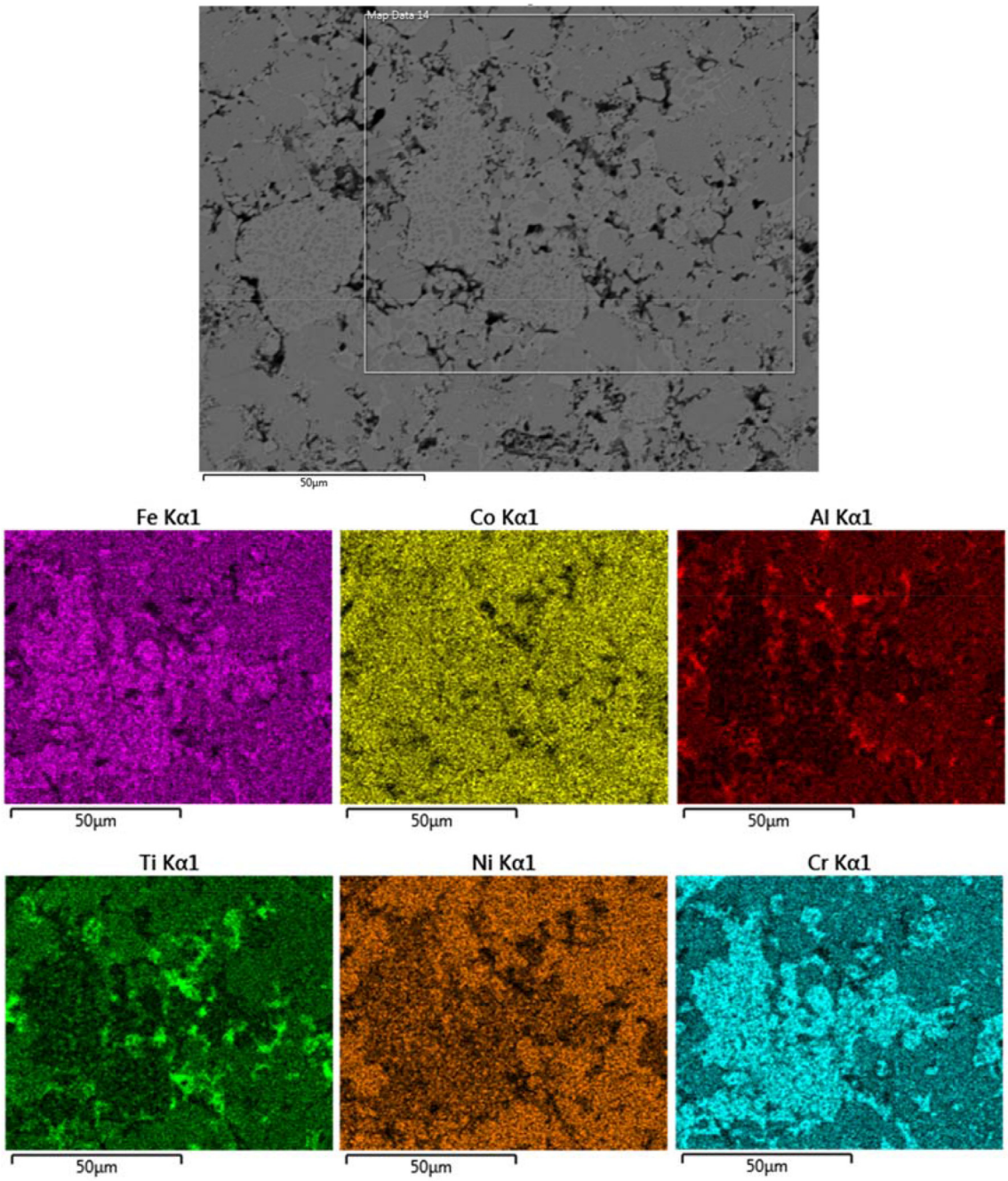

Fig. 4. SEM-MAP Analyses of as sintered $CoCrFeNiAl_{0.5}Ti_{0,5}$ sample.

Table 4
Chemical compositions of the as-sintered $CoCrFeNiAl_xTi_y$ alloys in atomic percentage.

Alloys	Region	Co	Cr	Fe	Ni	Al	Ti
$CoCrFeNiAl_{0.5}$	Dark(1)	14–20	3–10	13–18	21–30	15–30	–
	Light(2)	16–24	38–44	35–40	3–6	4–10	–
$CoCrFeNiAl_{0.5}Ti_{0.5}$	Dark(1)	16–18	12–19	16–21	18–25	7–11	7–11
	Light(2)	18–20	27–31	26–29	11–15	3–5	3–5
$CoCrFeNiAl_{0.5}Ti$	Dark(1)	11–16	7–9	12–18	19–23	15–17	29–34
	Light(2)	8–11	25–30	30–32	12–15	3–6	3–6
$CoCrFeNiTi_{0.5}$	Dark(1)	10–12	65–72	5–10	3–5	–	2–3
	Light(2)	18–21	28–35	17–22	15–18	–	12–15
	Mix(3)	9–11	5–7	9–10	13–15	–	56–58
$CoCrFeNiAlTi_{0.5}$	Dark(1)	8–14	3–6	8–10	15–23	18–27	18–23
	Light(2)	13–20	20–26	17–23	8–10	12–15	8–14

in alloy. And the lattice parameters of these phases are higher than those determined in the $CoCrFeNiAl_{0.5}Ti_{0.5}$ alloy. The increase in the weight ratio of Al and Ti in alloys with high atomic radius caused the increase of the lattice parameters. Absence of Al with high atomic radius in the $CoCrFeNiTi_{0.5}$ alloy leads that the peaks of the FCC phase are similar to the $CoCrFeNiAl_{0.5}$ alloy. Diffraction peaks were also determined in sigma phase and BCC1 in the alloy. In the $CoCrFeNiAlTi_{0.5}$ alloy, BCC1 and BCC2 phases were detected as in the compositionally similar $CoCrFeNiAl_{0.5}Ti$ alloy. According to XRD analysis, when the total atomic ratio of atoms such as Al and Ti having a high atomic radius exceeds 0.5, it can be seen that these elements stabilize the BCC instead of the FCC phase in the structure. This result has already been determined in some studies [11,13,32].

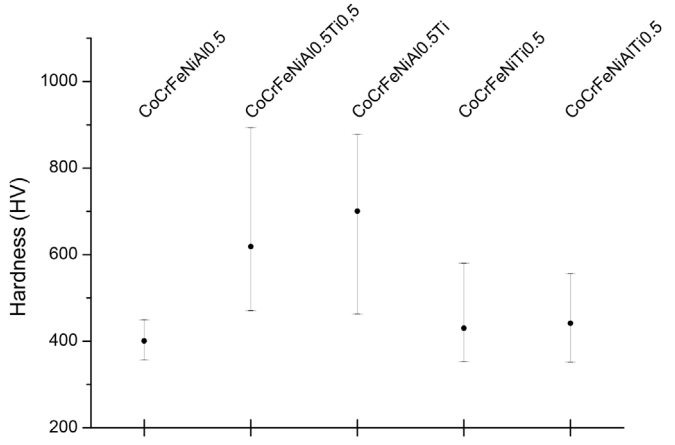

Fig. 5. Hardness variation graphs of as sintered samples.

3.2. SEM-EDS analyses of as-sintered CoCrFeNiAlxTiy alloys

Fig. 3, shows the SEM images of as-sintered $CoCrFeNiAl_xTi_y$ alloys. By SEM analyses, a characteristic microporous microstructure of sintered materials is observed. The black spots on the structure can be attributed to the aluminum oxide and the small amount of porosity surrounding it. Despite the total 5 min process time, pure metallic powders transformed to simple solid solutions and intermetallic phases at the end of the process. The chemical compositions of the phases were measured by EDS microanalysis in the SEM. SEM-map analyses were also conducted as it can be seen in Fig. 4. When the elemental distribution is examined in general, Al-Ni-Ti elements are enriched in dark phases while Fe-Cr elements are enriched in light color phases (Table 4). The large negative mixing enthalpy values between Ti, Ni and Al facilitate the formation of Al-Ni-Ti rich phase and the Fe-Cr rich phase subsequently precipitate around the Al-Ni-Ti rich phase due to high concentrations of Fe and Cr [9]. Co is distributed throughout the microstructure in homogeneous manner. This is attributed to the mixing enthalpies of the constituent binary alloys. For $CoCrFeNiAl_xTi_y$ alloys, the mixing enthalpies between Al and Co, Cr, Fe, Ni and Ti are −19, −10, −11, −22 and −30 kj/mol respectively; whereas the mixing enthalpies between Ti and Co, Cr, Fe, Ni and Al are −28, −7, −17, −35 and −30 kj/mol respectively [33]. Thus Al attracts Ti-Ni and Ti attracts Al-Ni to dark regions. Also light regions are enriched with Fe and Cr. In $CoCrFeNiAl_{0.5}$ alloy (Fig. 3a) light areas are corresponds to BCC1 phase and dark areas are corresponds to FCC phase, in $CoCrFeNiAl_{0.5}Ti_{0.5}$ alloy (Fig. 3b) light areas are corresponds to BCC1 phase and dark areas are corresponds to BCC2 phase according to the XRD pattern shown in Fig. 2. In the CoCrFeNiAl0.5Ti0.5 alloy, the sigma phase is dispersed in very fine in the dark phase. It can be inferred that the two BCC phases of the $CoCrFeNiAl_{0.5}Ti$ alloy are Al–Ni–Ti rich BCC2 phase (dark phase in Fig. 3c) and Fe–Cr rich BCC1 phase (light phase in Fig. 3c). According to the XRD patterns shown in Fig. 2 and the EDS results presented in Table 4, in the $CoCrFeNiTi_{0.5}$ alloy (Fig. 3d) dark and light phases are supposed to be BCC1 phase and FCC phase, respectively. In $CoCrFeNiAlTi_{0.5}$ alloy the corresponding SEM-EDS analyses clearly reveals that the Fe–Cr rich areas are the BCC1 phase and the Al–Ni–Ti enriched regions are the BCC2 phase (Fig. 3e).

The high entropy alloys exhibit high hardness that varies widely according to the contents of the elements that compose them. However, the phases formed in the microstructure also have a significant effect on the hardness. Average hardness values of respectively 401 H V, 618 H V, 700 H V, 430 H V and 441 H V were obtained after sintering in $CoCrFeNiAl_{0.5}$, $CoCrFeNiAl_{0.5}Ti_{0.5}$, $CoCrFeNiAl_{0.5}Ti$, $CoCrFeNiTi_{0.5}$ and $CoCrFeNiAlTi_{0.5}$ alloys. Fig. 5 gives the hardness graph of the alloys. The high deviation seen in the error bar in the graph is attributed to the different hardness of the phases in the alloy. The hardness of the alloys is given as averages after measurement with the Vickers microhardness tester at different phases. Intermetallic phases showed high hardness values when solid solution phases had lower values. Since Al and Ti atoms have a higher atomic radius than other component elements, they cause distortion in both FCC and BCC lattice structures and increase alloy hardness. However, hardness is also significantly influenced by the hard based phases formed in the structure besides the distortion of the solid solutions contained in the alloy. The hardness in the $CoCrFeNiAl_{0.5}$ alloy is obtained by the solid solution hardening mechanism, while the presence of Al-Ni-Ti and sigma intermetallic phases in the $CoCrFeNiAl_{0.5}Ti_{0.5}$ and $CoCrFeNiAl_{0.5}Ti$ alloys provides a significant increase in their hardness. Intermetallic compounds are usually brittle and thus increases hardness but decreases ductility [3,9,34]. The hardness of the CoCrFeNiAl0.5Ti0.5 alloy is higher than CoCrFeNiAl0.5Ti alloy by a small margin, although it contained more intermetallic phase. Hardness in alloys is not only affected by intermetallic phases. Al and Ti elements have not only a larger radius than most other elements, but also stronger binding forces with other elements, therefore, the increased Al and Ti elements in alloys causes the larger lattice strain effect and strong binding force so enhancement of hardness.

In the case of $CoCrFeNiTi_{0.5}$ alloy, the hardness is dominated by the hard sigma phase, which occurs in small quantities with distortion

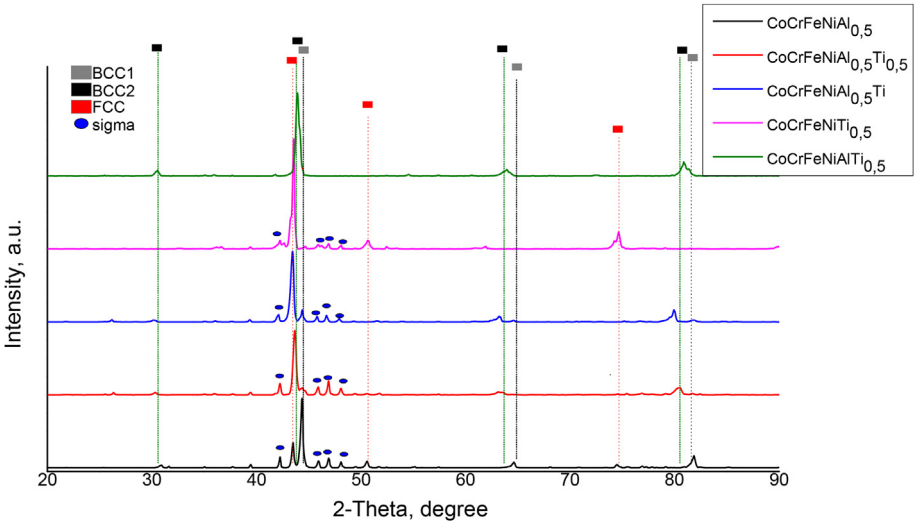

Fig. 6. XRD patterns of the as-homogenized $CoCrFeNiAl_xTi_y$ alloys.

Table 5
Phases and their lattice parameters of the as-homogenized $CoCrFeNiAl_xTi_y$ alloys, in accordance to the XRD analysis.

Alloy	Lattice	Lattice parameters (Å)
$CoCrFeNiAl_{0.5}$	BCC1 (FeCr) FCC (FeNi) Tetragonal (sigma)	2.885 ± 0.003 3.600 ± 0.003 a = 8.806 ± 0.005, c = 4.568 ± 0.003
$CoCrFeNiAl_{0.5}Ti_{0.5}$	BCC2 (Al-Ni-Ti) Tetragonal (sigma)	2.928 ± 0.003 a = 8.810 ± 0.006, c = 4.570 ± 0.003
$CoCrFeNiAl_{0.5}Ti$	BCC1 (FeCr) BCC2 (Al-Ni-Ti) Tetragonal (sigma)	2.882 ± 0.002 2.930 ± 0.003 a = 8.818 ± 0.004, c = 4.574 ± 0.003
$CoCrFeNiTi_{0.5}$	FCC (FeNi) Tetragonal (sigma)	3.596 ± 0.003 a = 8.809 ± 0.005, c = 4.570 ± 0.003
$CoCrFeNiAlTi_{0.5}$	BCC1 (FeCr) BCC2 (Al-Ni-Ti)	2.899 ± 0.002 2.913 ± 0.004

occurring in solid solition phases. Relatively low hardness value than expected is measured in the $CoCrFeNiAlTi_{0.5}$ alloy, that may e result from the presence of the Fe-Cr rich solid solution in the structure and the low ratio of intermetallic Al-Ni-Ti rich phase.

3.3. XRD analyses as-homogenized $CoCrFeNiAl_xTi_y$ alloys

XRD patterns of the as-homogenized alloys are shown in Fig. 6, and the identified phases with their lattice parameters are given in Table 5. After the homogenization process, in addition to the phases found after the sintering in the $CoCrFeNiAl_{0.5}$ alloy, it has been found that tetragonal structured sigma phase is also formed in the alloy. BCC1 phase observed after sintering was not detected while maintaining the presence of BBC2 and tetragonal crystal lattice structures in the $CoCrFeNiAl_{0.5}Ti_{0.5}$ alloy. In the XRD analysis after homogenization for $CoCrFeNiAl_{0.5}Ti$ alloy, it was determined that the tetragonal sigma phase dissociated from as-sintered alloy. In the $CoCrFeNiTi_{0.5}$ alloy, BCC1 is not seen in the structure but other phases are present. At the end of the homogenization process, similar phases were determined after sintering in general, and it was determined that the sigma phase dissociated or retained its presence in all alloys except $CoCrFeNiAlTi_{0.5}$ alloy. Further work on the formation of sigma phase in high entropy alloys is needed. No change in the post-sinter phase of the $CoCrFeNiAlTi_{0.5}$ alloy was observed except for the lattice parameters. The structure became more stable due to diffusion in the homogenization process. Therefore, it is seen that, after sintering, the lattice parameters determined at the end of homogenization generally increase.

3.4. SEM-EDS analyses of As- homogenized CoCrFeNiAlxTiy alloys

Fig. 7, presents the back scattered SEM micrographs and Table 6 outlines the chemical compositions of five considered homogenized alloys (analyzed by EDS). SEM-map analyses also were conducted as shown in Fig. 8. As a result of the homogenization, the chemical composition of the phases became more stable and the elemental scattering decreased. Similar to the $CoCrFeNiAl_{0.5}$, $CoCrFeNiAl_{0.5}Ti_{0.5}$ alloys, two main phases were observed in the microstructure; dark gray and light gray. In addition, these phases are dispersed in fine grains within each other. In $CoCrFeNiAl_{0.5}$ alloy, light areas correspond to BCC1 phase and dark areas correspond to FCC phase, in $CoCrFeNiAl_{0.5}Ti_{0.5}$ alloy light areas correspond to sigma phase and dark areas correspond to BCC2 phase according to the XRD pattern shown in Fig. 6. Due to the mixing enthalpy, the dispersion becomes more pronounced as a result of the homogenization process. In general, the Fe-Cr rich phase is precipitated due to its high concentration around this phase, while the large negative mixing enthalpy between Al-Ni-Ti elements facilitates the formation of Al-Ni-Ti rich phase during processing due to enthalpy values. Although Co is dispersed in mean values in most cases, it is slightly higher in the dark gray phase in the alloys having higher Al + Ti ratio, while is moderately higher in the light gray phase in the alloys having lower Al + Ti ratio. In $CoCrFeNiAl_{0.5}Ti$ alloy, three different phases are observed in microstructure as dark gray, gray and light gray, which correspond to BCC2, sigma and BCC1 phases respectively mentioned in the XRD analysis (see Fig. 6). The dark gray phase shows a composition similar to other alloys, while the gray and light gray phases are rich in Fe and Cr elements. Main difference between the gray and light gray phases is that the richest element Fe is in gray phase and Cr is in ligth gray phase. In the $CoCrFeNiTi_{0.5}$ alloy, when the matrix consists of dark gray phase (FCC), a light gray phase (sigma) dispersed in this matrix is seen in this matrix (Fig. 7). $CoCrFeNiAlTi_{0.5}$ exhibiting dark and light areas similar to those in $CoCrFeNiAl_{0.5}$, $CoCrFeNiAl_{0.5}Ti_{0.5}$ alloys which are confirmed to be the BCC2 and BCC1 phases, respectively according to the XRD pattern shown in Fig. 6.

Average hardness values of 496 H V, 956 H V, 916 H V, 673 H V and 753 H V were obtained after annealing in $CoCrFeNiAl_{0.5}$, $CoCrFeNiAl_{0.5}Ti_{0.5}$, $CoCrFeNiAl_{0.5}Ti$, $CoCrFeNiTi_{0.5}$ and $CoCrFeNiAlTi_{0.5}$ alloys, respectively (Fig. 9). The hardness values of all alloys increased with the homogenization process after the sintering process. This is related to two important factors. Particularly, formation of the hard-structured sigma phase has been found to contribute significantly to the hardness of alloys after homogenization. Stepanov et al. [8] studied the CoCrFeMnNiVx alloy and found that hardness of the alloys was greatly affected by the sigma phase. In many studies it has been previously determined that the sigma phase enhances the hardness of the alloys [35–37]. However, it has been determined that homogenization increases the lattice parameters of alloys. Due to this increase, the raising distortion in the lattice also contributed to the hardness. Furthermore, the presence of the Al-Ni-Ti rich intermetallic phase also enhances the hardness. Especially, the high hardness obtained in $CoCrFeNiAl_{0.5}Ti_{0.5}$, $CoCrFeNiAl_{0.5}Ti$ alloys is attributed to the presence of higher sigma and intermetallic phase ratio in the structure.

4. Conclusion

Microstructure and hardness properties of $CoCrFeNiAl_xTi_y$ high entropy alloys manufactured by the electric current activated sintered were studied in the as-sintered and homogenized at 1200 °C for 18 h conditions.

The following results can be derived from the present study:

- Thanks to the ECAS technique used in the study, HEAs production was conducted without using a protective atmosphere and was completed in as short time as 5 min.
- Achieved results are in agreement with the literature. In addition. This paper demonstrates superiority of HEA production in terms of short time processing compared to previous studies.
- Solid solution, intermetallic and sigma phases similar to those in the literature have been determined in this study. In addition, it has been found that the presence of Al and Ti elements having a high atomic radius in the composition has a positive effect on the hardness values depending on the phases formed.
- High hardness values are highly influenced by homogenization process and increased to 956 H V in the CoCrFeNiAl0.5Ti0.5 alloy due to the increase in distortion and high hardness sigma phase due to the increase of the lattice parameters.

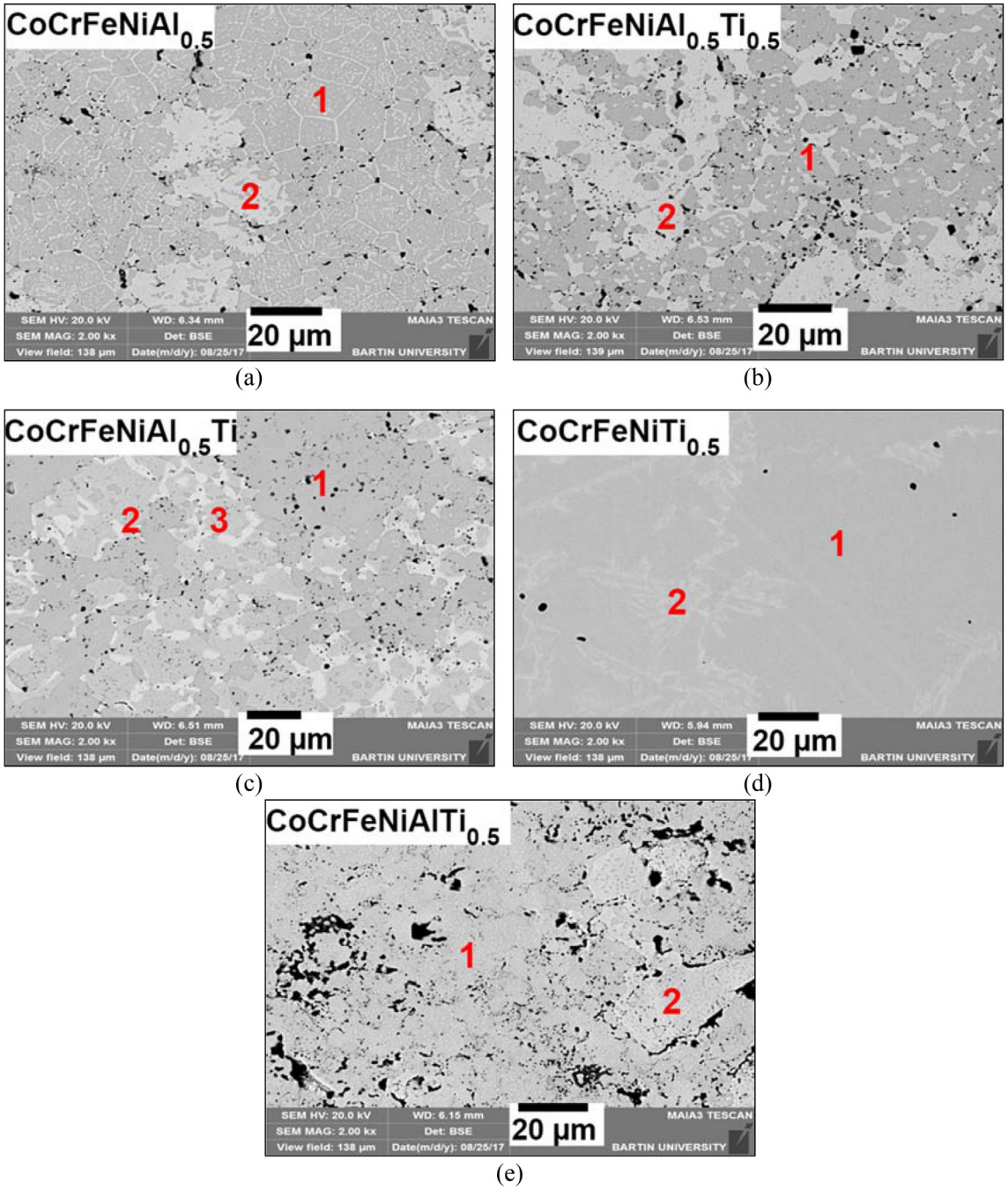

Fig. 7. SEM images of as-homogenized CoCrFeNiAlxTiy, (a) C1, (b) C2, (c) C3, (d) C4, (e) C5.

Table 6
Chemical compositions of the as-homogenized $CoCrFeNiAl_xTi_y$ alloys in atomic percentage.

Alloys	Region	Co	Cr	Fe	Ni	Al	Ti
$CoCrFeNiAl_{0.5}$	Dark(1)	19–21	11–13	16–18	29–31	17–19	–
	Light(2)	22–24	27–29	27–29	9–14	4–8	–
$CoCrFeNiAl_{0.5}Ti_{0,5}$	Dark(1)	23–24	8–9	11–13	27–29	13	13–14
	Light(2)	14–16	37–40	29–33	8–10	2.5	2–4
$CoCrFeNiAl_{0.5}Ti$	Dark(1)	23	6–7	11	26	12	22–23
	Gray (2)	7–8	47–48	32–33	6–7	1–2	3–4
	Light(3)	12–13	34–35	36–37	5–6	1–2	8–9
$CoCrFeNiTi_{0.5}$	Dark(1)	21–22	25–26	24–26	21–22	–	6–7
	Light(2)	20–21	25–26	26	21–22	–	5–6
$CoCrFeNiAlTi_{0.5}$	Dark(1)	19	15–16	19–20	19	18	9–10
	Light(2)	6–7	56–57	26–27	2–3	6	2

- As a result, it has been determined that with ECAS, very high entropy alloys can be produced together with many advantages in a very short time. It is aimed to continue the detailed studies on the identification of the phases and the examination of the mechanical and microstructural properties of the homogenization process.

Acknowledgement

The authors thank expert Murat Kazanci, technician Erkut Tas of Sakarya University for assisting with experimental studies. And a special thanks extends to Dr. Shafaqat Siddique from Dortmund Technical University for his notable support. This work was supported by Sakarya University Research Foundation (Project Number: 2015-50-02-037).

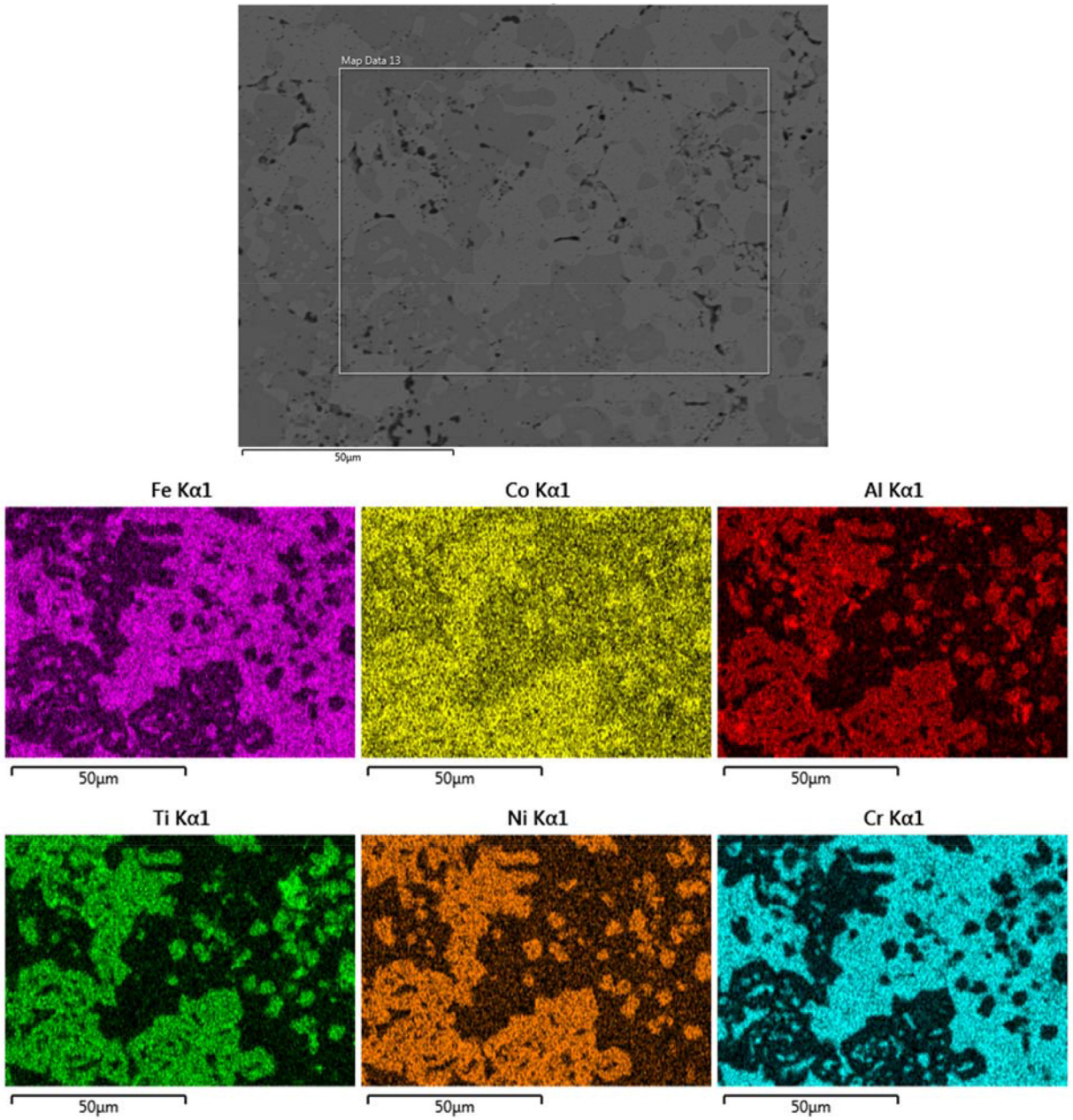

Fig. 8. SEM-MAP Analyses of as homogenized CoCrFeNiAl0.5Ti0,5 sample.

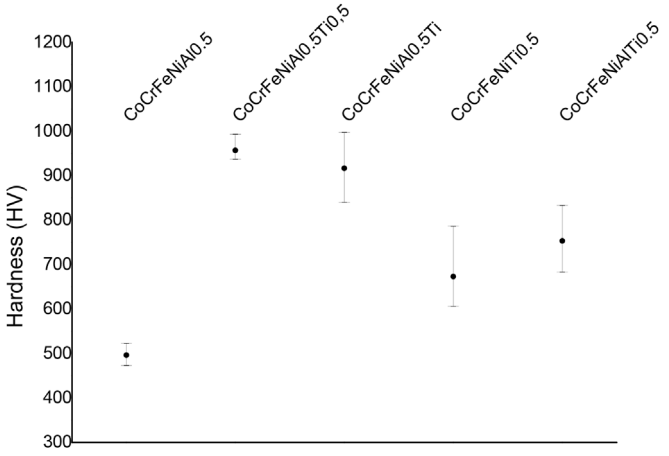

Fig. 9. Hardness variation graphs of as homogenized samples.

References

[1] Y. Zhang, T.T. Zuo, Z. Tang, M.C. Gao, K.A. Dahmen, P.K. Liaw, Z.P. Lu, Microstructures and properties of high-entropy alloys, Prog. Mater. Sci. 61 (2014) 1–93, http://dx.doi.org/10.1016/j.pmatsci.2013.10.001.

[2] M.-H. Tsai, J.-W. Yeh, High-entropy alloys: a critical review, Mater. Res. Lett. 2 (2014) 107–123, http://dx.doi.org/10.1080/21663831.2014.912690.

[3] W.H. Liu, J.Y. He, H.L. Huang, H. Wang, Z.P. Lu, C.T. Liu, Effects of Nb additions on the microstructure and mechanical property of CoCrFeNi high-entropy alloys, Intermetallics 60 (2015) 1–8, http://dx.doi.org/10.1016/j.intermet.2015.01.004.

[4] J. Zeng, C. Wu, H. Peng, Y. Liu, J. Wang, X. Su, Microstructure and microhardness of as-cast and 800 °C annealed AlxCr0.2Fe0.2Ni0.6-xand Al0.2Cr0.2FeyNi0.6-yalloys, Vacuum 152 (2018) 214–221, http://dx.doi.org/10.1016/j.vacuum.2018.03.035.

[5] Z. Cai, G. Jin, X. Cui, Y. Li, Y. Fan, J. Song, Experimental and simulated data about microstructure and phase composition of a NiCrCoTiV high-entropy alloy prepared by vacuum hot-pressing sintering, Vacuum 124 (2016) 5–10, http://dx.doi.org/10.1016/j.vacuum.2015.11.007.

[6] J.W. Yeh, S.K. Chen, S.J. Lin, J.Y. Gan, T.S. Chin, T.T. Shun, C.H. Tsau, S.Y. Chang, Nanostructured high-entropy alloys with multiple principal elements: novel alloy design concepts and outcomes, Adv. Eng. Mater. 6 (2004), http://dx.doi.org/10.1002/adem.200300567 299–303 + 274.

[7] B. Cantor, I.T.H. Chang, P. Knight, A.J.B. Vincent, Microstructural development in equiatomic multicomponent alloys, Mater. Sci. Eng., A 375–377 (2004) 213–218, http://dx.doi.org/10.1016/j.msea.2003.10.257.

[8] N. Stepanov, M. Tikhonovsky, N. Yurchenko, D. Zyabkin, M. Klimova, S. Zherebtsov, A. Efimov, G. Salishchev, Effect of cryo-deformation on structure and properties of CoCrFeNiMn high-entropy alloy, Intermetallics 59 (2015) 8–17, http://dx.doi.org/10.1016/j.intermet.2014.12.004.

[9] N.D. Stepanov, D.G. Shaysultanov, G.A. Salishchev, M.A. Tikhonovsky, E.E. Oleynik, A.S. Tortika, O.N. Senkov, Effect of v content on microstructure and mechanical properties of the CoCrFeMnNiVx high entropy alloys, J. Alloy. Comp. 628 (2015) 170–185, http://dx.doi.org/10.1016/j.jallcom.2014.12.157.

[10] Z. Wang, X. Wang, H. Yue, G. Shi, S. Wang, Microstructure, thermodynamics and compressive properties of AlCoCrCuMn-x (x = Fe, Ti) high-entropy alloys, Mater. Sci. Eng., A 627 (2015) 391–398, http://dx.doi.org/10.1016/j.msea.2015.01.002.

[11] Y. Yu, J. Wang, J. Li, H. Kou, W. Liu, Characterization of BCC phases in AlCoCrFeNiTix high entropy alloys, Mater. Lett. 138 (2015) 78–80, http://dx.doi.org/10.1016/j.matlet.2014.09.100.

[12] N. Nayan, G. Singh, S.V.S.N. Murty, A.K. Jha, B. Pant, K.M. George, U. Ramamurty, Hot deformation behaviour and microstructure control in AlCrCuNiFeCo high entropy alloy, Intermetallics 55 (2014) 145–153, http://dx.doi.org/10.1016/j.intermet.2014.07.019.

[13] Y.F. Kao, T.J. Chen, S.K. Chen, J.W. Yeh, Microstructure and mechanical property of as-cast, -homogenized, and -deformed AlxCoCrFeNi (0 ≤ x ≤ 2) high-entropy alloys, J. Alloy. Comp. 488 (2009) 57–64, http://dx.doi.org/10.1016/j.jallcom.2009.08.090.

[14] Z. Fu, W. Chen, H. Wen, Z. Chen, E.J. Lavernia, Effects of Co and sintering method on microstructure and mechanical behavior of a high-entropy Al 0.6 NiFeCrCo alloy prepared by powder metallurgy, J. Alloy. Comp. 646 (2015) 175–182, http://dx.doi.org/10.1016/j.jallcom.2015.04.238.

[15] Z. Fu, W. Chen, Z. Chen, H. Wen, E.J. Lavernia, Influence of Ti addition and sintering method on microstructure and mechanical behavior of a medium-entropy Al0.6CoNiFe alloy, Mater. Sci. Eng., A 619 (2014) 137–145, http://dx.doi.org/10.1016/j.msea.2014.09.077.

[16] K.B. Zhang, Z.Y. Fu, J.Y. Zhang, W.M. Wang, S.W. Lee, K. Niihara, Characterization of nanocrystalline CoCrFeNiTiAl high-entropy solid solution processed by mechanical alloying, J. Alloy. Comp. 495 (2010) 33–38, http://dx.doi.org/10.1016/j.jallcom.2009.12.010.

[17] F.J. Baldenebro-Lopez, J.M. Herrera-Ramírez, S.P. Arredondo-Rea, C.D. Gómez-Esparza, R. Martínez-Sánchez, Simultaneous effect of mechanical alloying and arc-melting processes in the microstructure and hardness of an AlCoFeMoNiTi high-entropy alloy, J. Alloy. Comp. 643 (2015) S250–S255, http://dx.doi.org/10.1016/j.jallcom.2014.12.059.

[18] F. Tian, L.K. Varga, N. Chen, J. Shen, L. Vitos, Empirical design of single phase high-entropy alloys with high hardness, Intermetallics 58 (2015) 1–6, http://dx.doi.org/10.1016/j.intermet.2014.10.010.

[19] Z. Chen, W. Chen, B. Wu, X. Cao, L. Liu, Z. Fu, Effects of Co and Ti on microstructure and mechanical behavior of Al0.75FeNiCrCo high entropy alloy prepared by mechanical alloying and spark plasma sintering, Mater. Sci. Eng., A 648 (2015) 217–224, http://dx.doi.org/10.1016/j.msea.2015.08.056.

[20] A. Gali, E.P. George, Tensile properties of high- and medium-entropy alloys, Intermetallics 39 (2013) 74–78, http://dx.doi.org/10.1016/j.intermet.2013.03.018.

[21] N.D. Stepanov, D.G. Shaysultanov, G.A. Salishchev, M.A.T, Structure and mechanical properties of a light-weight AlNbTiV high entropy alloy, Mater. Lett. 142 (2015) 153–155, http://dx.doi.org/10.1016/J.MATLET.2014.11.162.

[22] Z. Wang, M. Wu, Z. Cai, S. Chen, I. Baker, Effect of Ti content on the microstructure and mechanical behavior of (Fe36Ni18Mn33Al13)100-xTix high entropy alloys, Intermetallics 75 (2016) 79–87, http://dx.doi.org/10.1016/j.intermet.2016.06.001.

[23] Y. Sui, S. Gao, X. Chen, J. Qi, F. Yang, F. Wei, Y. He, Q. Meng, Z. Sun, Microstructures and electrothermal properties of AlxCrFeNi multi-component alloys, Vacuum 144 (2017) 80–85, http://dx.doi.org/10.1016/j.vacuum.2017.07.026.

[24] Y. Chen, S. Zhu, X. Wang, B. Yang, G. Han, L. Qiu, Microstructure evolution and strengthening mechanism of Al0.4CoCu0.6NiSix(x = 0–0.2) high entropy alloys prepared by vacuum arc melting and copper injection fast solidification, Vacuum 150 (2018) 84–95, http://dx.doi.org/10.1016/j.vacuum.2018.01.031.

[25] W. Ji, W. Wang, H. Wang, J. Zhang, Y. Wang, F. Zhang, Z. Fu, Alloying behavior and novel properties of CoCrFeNiMn high-entropy alloy fabricated by mechanical alloying and spark plasma sintering, Intermetallics 56 (2014) 24–27, http://dx.doi.org/10.1016/j.intermet.2014.08.008.

[26] R. Orrù, R. Licheri, A.M. Locci, A. Cincotti, G. Cao, Consolidation/synthesis of materials by electric current activated/assisted sintering, Mater. Sci. Eng. R Rep. 63 (2009) 127–287, http://dx.doi.org/10.1016/j.mser.2008.09.003.

[27] T. Yener, S. Siddique, F. Walther, S. Zeytin, Vpliv električnega toka pri izdelavi intermetalne zlitine niti s sintranjem, aktiviranim z električnim tokom, Mater. Tehnol. 49 (2015) 721–724, http://dx.doi.org/10.17222/mit.2014.161.

[28] T. Yener, S. Zeytin, Synthesis and characterization of metallic-intermetallic Ti-TiAl3, Nb-Ti-TiAl3 composites produced with Electric-Current-Activated Sintering (ECAS), Mater. Tehnol. 48 (2014) 847–850.

[29] A. Cordier, M. Kleitz, M.C. Steil, Welding of yttrium-doped zirconia granules by electric current activated sintering (ECAS): protrusion formation as a possible intermediate step in the consolidation mechanism, J. Eur. Ceram. Soc. 32 (2012) 1471–1477, http://dx.doi.org/10.1016/j.jeurceramsoc.2011.12.022.

[30] T. Yener, S.C. Okumus, S. Zeytin, In situ formation of Ti-TiAl 3 metallic-intermetallic composite by electric current activated sintering method, Acta Phys. Pol., A 127 (2015) 917–920, http://dx.doi.org/10.12693/APhysPolA.127.917.

[31] Y. Ye, X. Li, Z. Cheng, M. Zhang, S. Qu, The influence of sintering temperature and pressure on microstructure and mechanical properties of carbonyl iron powder materials fabricated by electric current activated sintering, Vacuum 137 (2017) 137–147, http://dx.doi.org/10.1016/j.vacuum.2016.12.044.

[32] J. Joseph, T. Jarvis, X. Wu, N. Stanford, P. Hodgson, D.M. Fabijanic, Comparative study of the microstructures and mechanical properties of direct laser fabricated and arc-melted AlxCoCrFeNi high entropy alloys, Mater. Sci. Eng., A 633 (2015) 184–193, http://dx.doi.org/10.1016/j.msea.2015.02.072.

[33] A. Takeuchi, A. Inoue, Classification of bulk metallic glasses by atomic size difference, heat of mixing and period of constituent elements and its application to characterization of the main alloying element, Mater. Trans. 46 (2005) 2817–2829, http://dx.doi.org/10.2320/matertrans.46.2817.

[34] Q.C. Fan, B.S. Li, Y. Zhang, Influence of Al and Cu elements on the microstructure and properties of (FeCrNiCo)AlxCuy high-entropy alloys, J. Alloy. Comp. 614 (2014) 203–210, http://dx.doi.org/10.1016/j.jallcom.2014.06.090.

[35] S.M. Dubiel, J. Cieślak, Sigma-phase in Fe-Cr and Fe-V alloy systems and its physical properties, Crit. Rev. Solid State Mater. Sci. 36 (2011) 191–208, http://dx.doi.org/10.1080/10408436.2011.589232.

[36] C.-C. Hsieh, W. Wu, Overview of intermetallic sigma (σ) phase precipitation in stainless steels, ISRN Metall 2012 (2012) 1–16, http://dx.doi.org/10.5402/2012/732471.

[37] Y.H. Jo, W.-M. Choi, S.S. Sohn, H.S. Kim, B.-J. Lee, S. Lee, Role of brittle sigma phase in cryogenic-temperature-strength improvement of non-equi-atomic Fe-rich VCrMnFeCoNi high entropy alloys, Mater. Sci. Eng., A 724 (2018) 403–410, http://dx.doi.org/10.1016/j.msea.2018.03.115.